

Piezoelectric Strain FET (PeFET) based Non-Volatile Memories

Niharika Thakuria, *Student Member, IEEE* and Sumeet K. Gupta, *Senior Member, IEEE*

Abstract— We propose non-volatile memory (NVM) designs based on Piezoelectric Strain FET (PeFET) utilizing a piezoelectric/ferroelectric (PE/FE such as PZT) coupled with 2D Transition Metal Dichalcogenide (2D-TMD such as MoS₂) transistor. The proposed NVMs store bit information in the form of polarization (P) of the FE/PE, use electric-field driven P -switching for write and employ piezoelectricity induced dynamic bandgap modulation of 2D-TMD channel for bit sensing. We analyze PeFET with COMSOL based 3D modeling showing that the circuit-driven optimization of PeFET geometry is essential to achieve effective hammer-and-nail effect and adequate bandgap modulation for NVM read. Our results show that distinguishability of binary states to up to 11X is achieved in PeFETs. We propose various flavors of PeFET NVMs, namely – (a) high density (HD) NVM featuring a compact access-transistor-less bit-cell, (b) 1T-1PeFET NVM with segmented architecture, targeted for optimized write energy and latency and (c) cross-coupled (CC) NVM offering a trade-off between area and latency. PeFET NVMs offer up to 7X smaller cell area, 66% lower write energy, 87% lower read energy and 44% faster read compared to 2D-FET SRAM. This comes at the cost of high write latency in PeFET NVMs, which can be minimized by virtue of optimized PE geometry.

Index Terms— Ferroelectric, non-volatile memory, piezoelectric, strain, transition metal dichalcogenides

I. INTRODUCTION

In the current era of machine learning, the requirements for data processing and storage have exploded [1]. Along with technology scaling, increasing the number of processing cores has been a viable solution for this situation [2]. State-of-the-art processors comprise of CMOS SRAM based cache which suffer from limited scaling capability and high static leakage, leading to gaps in bridging processor-memory performance. A memory that is fast, energy efficient, highly compact and has zero standby leakage is recommended for the evolving needs.

Emerging non-volatile memories (NVM) such as spin-memories [3], resistive RAMs [4], Phase Change Memories [5], ferroelectric (FE) based memories [6]–[9] address concerns of standby leakage. However, most of them [3]–[5] rely on current-driven write, which is slow and energy-hungry. An exception to this is FE-based NVMs employing low power electric-field (E) driven write. However, existing FE-based designs suffer from limitations such as destructive read in FERAMs, retention/variability concerns in FEFETs and gate leakage in

This paper was submitted on January 10, 2022 and accepted on xx, 2022. This research was supported by Army Research Office (W911NF-19-1-048).

Thakuria and Gupta are with the School of Electrical and Computer Engineering, Purdue University ({nthakuri, guptask}@purdue.edu).

FE-Metal-FETs (FEMFET) [6], [8], [9]. Hence, a natural question is if an NVM can be designed to retain useful features of FE (e.g., E -driven write) while alleviating the said concerns.

Recently, a steep switching device was proposed which employs electrostrictive or piezoelectric (PE) effect of materials such as PMN-PT in conjunction with 2D Transition Metal Dichalcogenides (2D-TMD) FETs [10] to achieve sub-60mV/decade sub-threshold swing. Motivated by the unique operation of this device, we propose an NVM device which utilizes PE/FE material (such as PZT-5H) coupled with 2D-TMD FET (such as MoS₂) to tackle issues in FE-based NVMs.

The proposed piezoelectric strain FET (PeFET) based NVM features (a) FE polarization (P)-based bit-storage (b) E -driven write and (c) coupling of piezoelectricity of FE with dynamic bandgap (E_G) tuning of 2D-TMD for read [11]. PeFET inherits the advantages of FE and 2D-TMDs (such as scalability and enhanced gate control [10]). It leverages unique coupling of PE/FE with 2D-TMD for designing NVMs that can mitigate challenges associated with FE-based NVMs. Due to its unique structure and operational mechanism, the proposed PeFET NVM can potentially achieve (i) retention as high as FERAMs (the highest amongst all FE NVMs), (ii) non-destructive read and (iii) elimination of the gate leakage concerns due to absence of any floating metal layers. However, the benefits of PeFETs are accompanied by certain device limitations, which we tackle at the circuit/array level by pursuing a device-circuit co-design approach. With this in view, we propose multiple PeFET based NVMs. Our contributions in this manuscript are as following:

1. We present Piezoelectric Strain FET (PeFET), which utilizes P -based bit storage in PZT-5H, E -driven P -switching, and piezoelectricity induced dynamic bandgap modulation in 2D-TMD (MoS₂) channel for bit sensing.
2. We propose PeFET NVMs namely, High Density (HD), 1T-1PeFET and cross-coupled (CC) cell. HD is targeted for high density memories while the latter two for low power write.
3. We conduct an extensive device-circuit co-design to establish the design requirements and area-energy-latency tradeoffs of PeFET NVMs with respect to 2D-FET SRAMs.

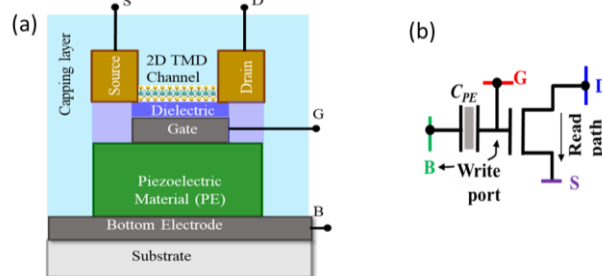


Fig. 1: (a) Device structure (b) schematic of PeFET.

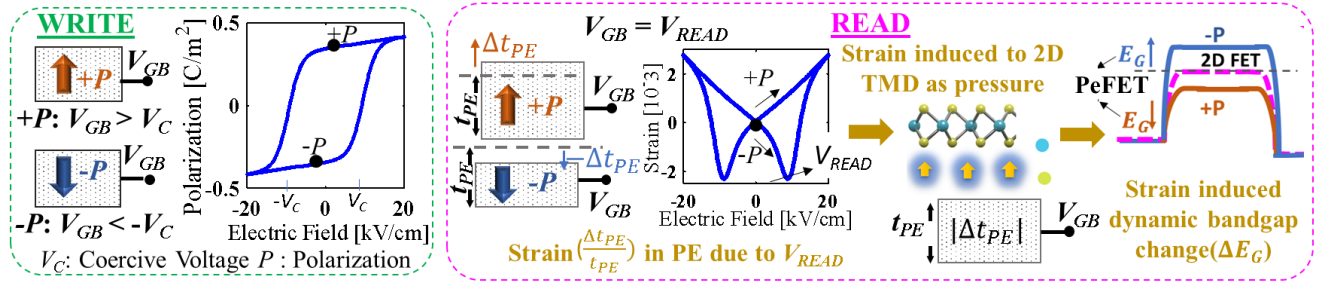


Fig. 2: Write and read operation of PeFET.

II. BACKGROUND

A. Ferroelectric (FE) based NVMs

The ferroelectric RAM or FERAM is among the earliest NVM that utilized low power electric-field driven write. FERAM had garnered interest due to its highly compact 1 transistor-1 capacitor (1T1C) cell configuration and high retention (due to lower depolarization fields compared to FEFETs). However, a drawback of this design is destructive read which requires write-back and leads to read inefficiencies. On the other hand, FEFETs offering separate read-write paths overcome the issue of destructive read. Two flavors of FEFETs have been explored (a) with an inter-layer metal (ILM) between FE and the underlying transistor (also called FEMFET) and (b) without an ILM i.e. with FE integrated directly on the channel or the gate dielectric (DE). FEFET without ILM features polarization-induced threshold voltage shift, which can be utilized to sense the stored data. While offering useful features such as multi-level storage and compact 1T design [13], FEFETs without ILM need high write voltage and suffer from variability, endurance and retention concerns due to traps at the FE-DE interface and depolarization fields in the FE. On the other hand, FEFETs with ILM exhibit mitigation of some of these issues because (a) the ILM decouples the cross-sectional optimization of FE and the underlying transistor, which helps in write voltage reduction [8] and (b) the ILM between FE and DE reduces traps and related issues. However, the presence of a floating ILM makes this device vulnerable to gate leakage, which leads to severe bit sensing challenges [9]. Furthermore, NVMs based on FEFETs with ILM typically require one or more access transistors (e.g. 2T/3T/4T designs [22]) to selectively access cells in an array, reducing their integration density. In the proposed PeFETs, we attempt to overcome some of the cited limitations of FE-based NVMs while exploiting low-power E -driven write in FE. As described later, the unique piezoelectricity-induced bandgap modulation based read in PeFETs enables a four-terminal device design with gate, drain, source and back contacts. They serve as knobs to discretely control read-write paths, enabling non-destructive read. The absence of floating metal in this device eliminates gate leakage concerns. Further, the PE layer is controlled by metals on both its sides, alleviating the issues of traps, variability and retention.

B. Piezoelectric (PE) based devices

An important design consideration for PeFET is the choice of PE material. We envision utilization of both ferroelectric and piezoelectric properties of PE material in this device. To this end, PZT-5H is one of the suitable materials as it possesses (i) sufficiently wide hysteresis of polarization-voltage response for

non-volatility and (ii) large enough strain for achieving effective bandgap modulation in 2D-TMD. This is different from the previous proposals of PE based FETs, e.g., PiezoElectronic Transistor (PET) [14] and Electrostrictive FET (EFET) [10] that were designed as steep-switching/logic devices. Hence, large piezoelectric coefficient is the primary requirement for the PE material in these devices. They utilize PMN-PT to modulate the resistance of piezoresistive material in PET [14] or bandgap of 2D-TMD channel in EFET [10]. However, PMN-PT is not ideal for the proposed NVM due to its low coercive field despite its impressive piezoelectricity.

Another important aspect of PeFET is that the 2D-TMD in the channel should allow sufficient piezoelectricity induced bandgap modulation. Various experiments have demonstrated monotonic bandgap reduction in 2D-TMD, especially MoS₂, on application of out-of-plane pressure. For example, monolayer MoS₂ achieves bandgap reduction of up to ~800meV/GPa [11]. EFET proposed in [10] discusses modulation of MoS₂ with piezoelectricity induced out-of-plane pressure in the context of logic applications. We extend the idea of piezoelectricity driven bandgap modulation of 2D-TMD to NVM design [15]. Our PeFET NVM stores bit information in PE and leverages polarization-dependent piezoelectric response to modulate the bandgap of mono-layer MoS₂ for sensing.

III. PIEZOELECTRIC FET (PEFET) DESIGN AND MODELING

A. Device structure and operation

PeFET consists of four terminals, namely drain (D), gate (G), source (S) and back (B) contacts (Fig. 1). A piezoelectric (PE) material (which also exhibits ferroelectricity) sits between G and B . The bit is stored in the form of polarization (P) in PE, with $+(-)P$ representing logic '1' ('0') (Fig. 2). Application of voltage across G and B (V_{GB}) enables writing states 1/0 to PE by switching P . V_{GB} greater than coercive voltage of PE (V_C) leads to $+P$ in the PE, while $V_{GB} < -V_C$ yields $-P$ storage.

In addition to write, G plays an important role in sensing of the PeFET states. It is used to generate P -dependent piezoelectric behavior in PZT. Moreover, it electrostatically controls the 2D-TMD channel (monolayer MoS₂). A positive read voltage (V_R) is applied to G such that $0 < V_R < V_C$. Such V_R creates strain in PE (S_{PE}) [16] by modulating its thickness (Δt_{PE}) based on the stored P (Fig. 2). For $+P$, PE thickness extends, i.e., $\Delta t_{PE} > 0$ and $S_{PE} > 0$; while $-P$ results in shrinking of PE thickness, $\Delta t_{PE} < 0$ and $S_{PE} < 0$ (Fig. 2). Consequently, S_{PE} yields a positive or negative stress in PE (σ_{PE}). σ_{PE} transduces as pressure in TMD (σ_{TMD}). σ_{TMD} causes dynamic modulation in the bandgap (ΔE_G) of TMD [11] (Fig. 2). If $\sigma_{TMD} > 0$ (resulting from $S_{PE} > 0$ or $+P$), $\Delta E_G < 0$ and bandgap

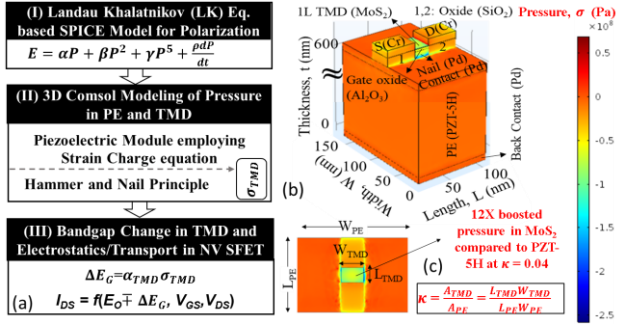


Fig. 3: (a) Simulation framework of PeFET, (b) 3D Modeling of PeFET in COMSOL Multiphysics, (c) Effect of ‘hammer-and-nail’ on PeFET showing boosted pressure in TMD.

reduces. Otherwise, when $\sigma_{TMD} < 0$ (for $S_{PE} < 0$ or $-P$), $\Delta E_G > 0$ and bandgap is higher. The effect of ΔE_G reflects in drain current (I_{DS}) as low/high resistance states (LRS/HRS) (Fig. 2). For $+P$, $S_{PE} > 0$, $\Delta E_G < 0$ and $I_{DS} = I_{LRS}$ (high) and $-P$ yields $S_{PE} < 0$, $\Delta E_G > 0$ and low $I_{DS} = I_{HRS}$ (Fig. 5(b)).

To efficiently transduce σ_{PE} to σ_{TMD} , we utilize hammer and nail effect, similar to [14], wherein the area of 2D-TMD above the gate (A_{TMD}) acts as the nail while PE serves as the hammer (Fig. 3(b)). We design A_{TMD} to be smaller than the area of PE (A_{PE}) by choosing appropriate PE dimensions. Note that A_{TMD} is fixed by the feature size (F) and width (W) of PeFET. In our design, we choose $F=20\text{nm}$ and $W=30\text{nm}$ (minimum width for high integration density). We select metals with high stiffness for the nail, PE and source/drain contacts (e.g., Pd, Cr) and encapsulant surrounding the device to minimize loss of σ_{PE} . The purpose of the encapsulant is to provide favorable boundary conditions for stress to be maximized at the TMD channel.

B. Modeling

We develop a simulation framework shown in Fig. 3 to analyze the proposed PeFET. We model P - E response of PZT-5H using Landau-Khalatnikov (LK) equation [17] and calibrate it with experimental data in [16]. Further, we model pressure transduced from PE to 2D-TMD (σ_{TMD}) using COMSOL Multiphysics Suite. We simulate 3D structure of PeFET (including hammer and nail effect) in COMSOL and employ strain-charge form of the constitutive equations for PE to obtain σ_{PE} and σ_{TMD} . We use boundary conditions on the top surface of the device (over the contacts and TMD) that represent a stiff encapsulant material. The piezoelectric coefficients (d_{33} and d_{31}) of PZT-5H for this simulation are extracted from experimentally obtained S - E response in [16]. σ_{TMD} is converted to ΔE_G using reported bandgap coefficient (α) for mono-layer MoS₂ [11]. ΔE_G is self-consistently coupled with Verilog-A based 2D-TMD FET model [18] by accounting for impact of dynamically changing bandgap on charge/potential of 2D-TMD channel. The 2D-TMD FET model provides P -dependent I_{DS} of PeFET, and is used in HSPICE to design the NVMs. The

$\alpha = -3.95\text{e6m/F}$	$\beta = 1.26\text{e6m}^5/\text{F/C}^2$	$\gamma = 3.21\text{e8m}^9/\text{F/C}^4$
$d_{33} = 650\text{pm/V}$	$d_{31} = -320\text{pm/V}$	$\mu_{TMD} = 90\text{cm}^2/\text{Vs}$
$R_C = 200\Omega\text{-}\mu\text{m}$	$\alpha_{TMD} = 806\text{eV/GPa}^{-1}$	$E_0 = 1.5\text{eV}$
$t_{PE} = 600\text{nm}$	$t_{nail} = 10\text{nm}$	$tox = 3\text{nm}$
$t_{TMD} = 0.65\text{nm}$	$L_G = 20\text{nm}$	$W_{TMD} = 30\text{nm}$

Fig 4: Parameters used for simulation

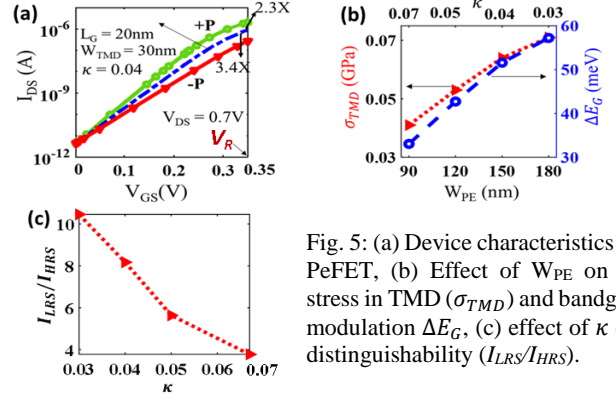


Fig. 5: (a) Device characteristics of PeFET, (b) Effect of W_{PE} on κ , stress in TMD (σ_{TMD}) and bandgap modulation ΔE_G , (c) effect of κ on distinguishability (I_{LRS}/I_{HRS}).

parameters used are based on experiments or reported literature [14], [16], [19], [20] and summarized in Fig. 4.

C. Device characteristics

Let us start by understanding the strain transduction characteristics of the PeFET. Our results from COMSOL simulations (Fig. 3(b)) show that the hammer and nail effect boost σ_{TMD} compared to σ_{PE} , when the area of nail/2D-TMD (A_{TMD}) is smaller than that of PE (A_{PE}), the hammer. The device parameter $\kappa = A_{TMD}/A_{PE}$ is a measure of this effect [14], where smaller κ is expected to provide larger σ_{TMD} . We observe $\sim 12\text{X}$ increase in σ_{TMD} compared to σ_{PE} at $\kappa = 0.04$ (Fig. 3(c)). We will explain the effect of κ in more detail in the next sub-section.

Let us now discuss polarization/strain-dependent transfer characteristics (I_{DS} - V_{GS}) of PeFET (Fig. 5(a)) with $\kappa = 0.04$. To avoid P -switching, we apply gate voltage (V_G) $< V_C$ of PZT-5H ($= 0.6\text{V}$ at PE thickness of 600nm), while keeping back voltage (V_B) = 0. For comparison, we also simulate a baseline device with $V_{GB}=0$ (i.e. with V_G and V_B swept together), from which we obtain P -independent nominal transfer characteristics of MoS₂-FET. Our results show at $V_{GS} = 0.35\text{V}$, $+P$ state in the PeFET yields $\sigma_{TMD} = 0.64\text{GPa}$ and $\Delta E_G = 51\text{meV}$ causing 2.3X higher I_{DS} (I_{LRS}). While, $-P$ results in 3.4X lower I_{DS} (I_{HRS}) at $V_{GS} = 0.35\text{V}$ compared to baseline.

Based on I_{DS} - V_{GS} characteristics, we identify that $0.3\text{V} < V_{GS} < 0.4\text{V}$ provides optimal distinguishability (I_{LRS}/I_{HRS}), necessary current for read operation and ample read disturb margin ($V_C - V_{GS} \sim 200\text{mV}$). We choose $V_{GS} = V_R = 0.35\text{V}$ which leads to $I_{LRS}/I_{HRS} \sim 8\text{X}$ (Fig. 5(c)) at $\kappa = 0.04$. Note that I_{LRS}/I_{HRS} can be improved by device optimization (e.g. by reducing κ), which we discuss in the next sub-section.

D. κ analysis

Lower κ boosts stress in TMD due to ‘hammer and nail effect’. κ tuning is achieved by appropriately choosing the PE width (W_{PE}), and thereby A_{PE} (Fig. 5(b)). This leads to a design time optimization of σ_{TMD} and ΔE_G . By increasing W_{PE} from 90nm to 180nm , κ decreases from 0.07 to 0.03 , leading to 1.78X increase in σ_{TMD} and ΔE_G (Fig. 5(b)). Hence, for $+P$, more aggressive bandgap reduction is observed at small κ , increasing I_{LRS} . Whereas in $-P$, bandgap increases with a decrease in κ , which weakens I_{HRS} . Strong I_{LRS} combined with weak I_{HRS} increases I_{LRS}/I_{HRS} and hence distinguishability from 3X to 11X as κ is reduced from $0.07 - 0.03$ (Fig. 5(c)).

IV. PEFET BASED NON-VOLATILE MEMORY DESIGNS

With the understanding of the device operation of PeFETs, we now propose three flavors of PeFET-based NVMs, namely, high density (HD), 1T-1PeFET and cross-coupled (CC) cells.

A. High density (HD) Non-Volatile Memory

HD NVM is designed with 1-PeFET, without an access-transistor (Fig. 6(a, b)). G of PeFET is connected to word line (WL) that is shared along a row. B and D are connected to write bit-line (WBL) and read bit-line (RBL) respectively, (Fig. 6(c)) and are shared along a column. Notice that B is being shared by adjacent cells in a column (Fig 6(b)) which helps in minimizing area. Next, we discuss the write and read operations.

1. Write: WL and WBL , connected in cross-point fashion, form the write port with C_{PE} between them [Fig. 6(c)]. To write, WBL and WL of the accessed cells are asserted such that $|V_{GB}| = V_{DD} > V_C$ appears across PE, resulting in P switching. We implement a two phase write operation to enable writing the states ‘1’ and ‘0’ in different cells of a word (in the same row). To write ‘1’, we drive WBL to $-V_{DD}/2$. Next, we drive WL to $-V_{DD}/2$ in phase one (Φ_1) and switch to $V_{DD}/2$ in the second (Φ_2). Consequently, $V_{GB} = V_{WL} - V_{WBL} = 0$ in Φ_1 which has no effect on P and $V_{GB} = V_{WL} - V_{WBL} = V_{DD}$ causes PE to switch to $+P$ (‘1’) in Φ_2 . Similarly, ‘0’ is written by driving WBL to $V_{DD}/2$ and asserting WL like before. Now, $V_{GB} = V_{WL} - V_{WBL} = -V_{DD}$ switches polarization to $-P$ in Φ_1 and $V_{GB} = 0$ retains $-P$ in Φ_2 .

With write using $\pm V_{DD}/2$ for accessed cells, $WBLs/WLs$ of half-accessed/un-accessed cells can be kept at 0V. Hence, half-accessed cells experience $|V_{GB}| \leq V_{DD}/2 < V_C$, and un-accessed cells have $V_{GB} = 0$, thereby averting write disturbs. Having BL/WL of half-accessed/un-accessed at 0V cuts down write energy that may be present in other cross-point architectures based on $V_{DD}/2$ or $V_{DD}/3$ biasing for half/un-accessed cells [21].

Note that due to absence of access transistors (AX), use of negative voltages for write does not incur large energy overheads compared to previous designs based on other technologies involving AX [22]. In latter designs, negative write voltage also needs to ensure WLs of all the unaccessed rows are driven to negative voltage to avert their turning ON. This incurs a significant energy cost, which is absent in HD design. For the same reason, in our other PeFET designs that employ AX, we constrain write biasing voltage to be positive (details later).

2. Read: We apply $V_R (=V_{DD}/2 < V_C)$ on WL and V_{DD} to RBL of accessed cells. Read current is sensed on RBL in a single phase. Half accessed rows have WL at 0V while in half accessed columns, RBL voltage is 0V. Hence, current flow through half-accessed/unaccessed cells is negligible or zero.

The lack of AX in HD cells and sharing of back contact in the layout results in a compact design. However, absence of AX

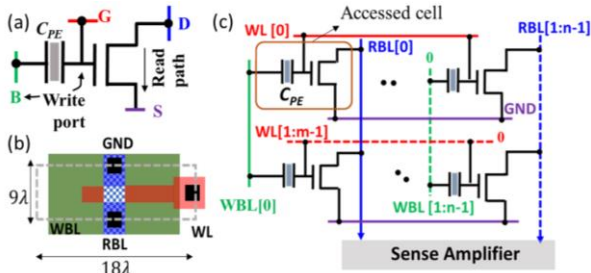


Fig. 6 (a) Schematic (b) Layout and (c) Array of HD PeFET

exposes PE capacitance (C_{PE}) of half-accessed cells directly on WBL . Since C_{PE} is typically large (dielectric constant $\sim 4000\epsilon_0$), write energy efficiency is adversely affected. Based on our analysis, we attribute that 78% of write energy is originated from charging/discharging of C_{PE} , followed by 12% due to metal capacitance switching of BLS/WL and 10% due to P -switching. To minimize effect of C_{PE} on write energy, we propose PeFET NVMs with AX that isolates WBL from C_{PE} .

B. 1T-1PeFET Non-Volatile Memory [Fig.7(a)]

1T-1PeFET consists of an n-type 2D FET connected to back contact (B) of a PeFET. Notice that unlike in HD NVM, large C_{PE} on WBL is replaced by smaller drain capacitance from AX in a column. We explore two variants of layout for this cell: (i) tall layout for area optimized design [Fig. 7(b)] and (ii) wide layout where the cell height is minimized [Fig. 7(c)]. The latter is motivated from our understanding that bit line capacitance is the dominating contributor for delay and energy in 1T-1PeFET arrays. For example, 79% of its total write energy is attributed to $V_{DD}/2$ switching of $WBLs$ in half-accessed cells. $WBLs$ of half-accessed cells must be driven to $V_{DD}/2$ to ensure $|V_{GB}| < V_C$ across their PEs in order to prevent P -switching. Such a requirement also causes a large overhead in write energy. To mitigate this, we present Segmented 1T-1PeFET NVM.

C. Segmented Architecture of 1T-1PeFET NVM

1T-1PeFET segmented architecture [Fig. 7(e)] which eliminates energy overheads from half-accessed/unaccessed cells is motivated by FERAM architecture [23].

The 1T-1PeFET segmented array is divided into multiple segments each comprising of 64 columns that correspond to size of a word (N_W) and N_R rows. If the entire array is constituted of N_C columns and N_R rows, there are $N (= N_C/N_W)$ segments, each of size $N_W \times N_R$. Moreover, global plate line (GPL) is responsible for the said segmentation. The array contains $N = N_C/N_W$ $GPLs$. $GPLs$ provides input to N_R buffers in each segment. These buffers act as gates for a segment and their output drives a local plate line (LPL). LPL connects the 64 cells ($= N_W$). Note that LPL is loaded with a smaller net C_{PE} from 64 cells instead of an entire row (as in a standard architecture). The WL , which runs through a row, provides supply voltage to the buffers and also activates the AXs of 1T-1PeFET NVMs in the accessed row. In addition, each column in a segment has its own WBL and RBL . In summary, each segment comprises of (i) a GPL , (ii) N_R $LPLs$, (iii) N_R WLs that are shared by other segments, (iv) N_W $WBLs$ and (v) N_W $RBLs$. Now, let us understand the implication of the segmented architecture on the write and read operations of 1T-1PeFET.

1. Write: Two phase signal, i.e., 0 (Φ_1) \rightarrow V_{DD} (Φ_2) is applied to GPL of the accessed segment during write. Write input data 0/ V_{DD} is provided to N_W $WBLs$. Let the first word of first segment (accessed word in Segment [0] of Fig. 7(e)) is to be written to, without any loss in generality. WL is asserted with $V_{DD} + V_{TH}$ which activates Buffer[0]. LPL of the accessed word ($LPL_0[0]$) is 0 and $V_{DD} + V_{TH}$ when GPL is 0 and V_{DD} respectively. If $WBL = 0$, $V_{GB} = 0$ in Φ_1 and $V_{GB} = V_{DD} + V_{TH}$ in Φ_2 . Hence, $+P$ state (logic 1) is written in Φ_2 . Similarly, if $WBL = V_{DD}$, $V_{GB} = -V_{DD}$ in Φ_1 and $-P$ state (logic 0) is being written. All $RBLs$ along with $WBLs$ and $GPLs$ of un-accessed words/segments (e.g., $GPL[1]$ to $GPL[N-1]$) are kept at 0V.

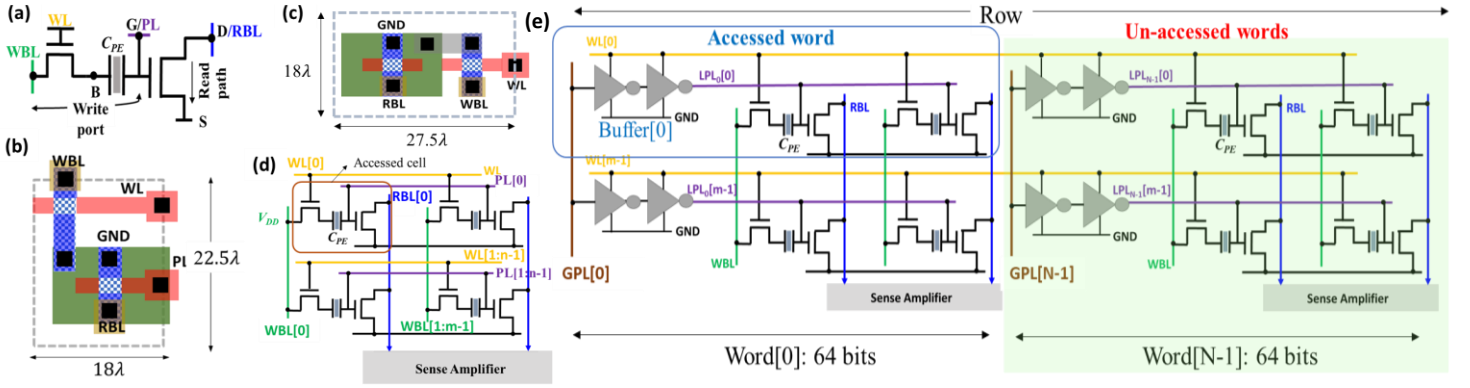


Fig. 7 (a) Schematic (b) tall layout (c) wide layout, (d) array and (e) segmented array of 1T-1PeFET

Hence, their LPL s are also at $0V$. Thus, energy expended by these segments is minimized in this architecture.

2. Read: We accomplish read by driving GPL of accessed segment and WL to V_R while keeping WBL s at 0 . This results in V_R on LPL (e.g., $LPL_0[0]$ in Fig. 7(e)). Read current is sensed with RBL voltage at V_{DD} . The voltages of GPL , WBL , RBL of un-accessed sections and WL of un-accessed rows are $0V$.

D. Cross-coupled PeFET NVM (CC) [Fig. 8(a)]

In 1T-1PeFET, we focused on design aspects that minimized impact of C_{PE} on cell performance and energy consumption. By applying segmentation, we further minimized the interaction of C_{PE} . However, a limitation of 1T-1PeFET is the area overhead added by AX. Also, unlike in HD cell, the back contact is an internal node in 1T-1PeFET that cannot be shared, constraining its compactness as per design rules. Furthermore, although reduced considerably, C_{PE} still needs to be switching during read. To alleviate the burden of C_{PE} during read while also targeting cell area reduction compared to 1T-1PeFET cells, we propose cross-coupled (CC) PeFET NVM cell. The technique of cross-coupling two PeFETs in this cell allows us to share the back-contact (along a row), thereby conserving cell area. Our layout analysis [Fig. 8(b)] suggests that the area per bit in CC is 1.36X and 1.66X lower than 1T-1PeFET tall and wide cell respectively at $\kappa = 0.04$. Moreover, the back contact (hence C_{PE}) need not be switched in CC NVM during read (remains at $0V$), thus improving read latency and energy.

We design CC cell [Fig. 8(a)] with two PeFETs (A and B) that are cross-coupled by connecting D of A (D_A) to G of B (G_B) and vice-versa. D_A and D_B are connected to bit-lines BL_1 and BL_2 respectively through AX_1 and AX_2 . G of AX_1/AX_2 are controlled by WL . Back contacts of A and B are driven by PL . Bits in A and B can be stored, read and written individually. Hence, each CC cell is equivalent to a 2-bit NVM.

E. Segmented Architecture of CC NVM (Fig. 9)

We propose segmentation in CC NVM array similar to 1T-1PeFET array so that PL has reduced C_{PE} load during write. Each segment comprises of (i) N_R rows, (ii) 32 columns of CC cells that effectively act as 64 bits of a word (N_W), (iii) a GPL that provides input to N_R buffers, that are in turn activated by a WL and (iv) N_R LPL s driven by the output of buffers. Notice that a LPL is a PL (back contact) shared horizontally by 32 CC cells within a segment. One key difference between 1T-1PeFET and CC segmented array is that the LPL voltage during read

needs to be switched to V_R in the former, while it is $0V$ in CC NVM. This eliminates the effect of C_{PE} during read for improved read latency and energy efficiency. Next, we explain the write and read operations in a segmented CC array.

1. Write: Here, we explain various cases of writing to A and B. When we intend to store complementary states to A and B, i.e., $+P$ (or $-P$) to A and $-P$ (or $+P$) to B, BL_1 and BL_2 are driven to $0V$ (or V_{DD}) and V_{DD} (or $0V$) respectively. 0 (Φ_1) $\rightarrow V_{DD}$ (Φ_2) is applied to GPL of selected segment and WL is asserted with $V_{DD} + V_{TH}$. LPL receives $0 \rightarrow V_{DD}$ as output. Moreover, voltage at BL_1 and BL_2 is passed to G_B and G_A respectively by CC NVM's AXs after WL assertion. For PeFET A, $V_{GB,A}$ ($V_{GB,A}$) = $V_{BL_2} - V_{LPL}$. Similarly, $V_{GB,B}$ ($V_{GB,B}$) is $V_{BL_1} - V_{LPL}$. Say, $V_{BL_1} = 0$, $V_{BL_2} = V_{DD}$ and LPL is signaled with 0 (Φ_1) $\rightarrow V_{DD}$ (Φ_2), then we get $V_{GB,A} = V_{BL_2} - V_{LPL} = V_{DD}$ in Φ_1 ; $+P$ is being written to A. For B, $V_{GB,B} = V_{BL_1} - V_{LPL} = -V_{DD}$ during Φ_2 which is when $-P$ is written.

To store $-P$ in both A and B, BL_1 and BL_2 are maintained at $0V$. After WL is asserted and $0 \rightarrow V_{DD}$ appears on LPL (like before), $V_{GB,A}/V_{GB,B} = -V_{DD}$ is obtained during Φ_2 switching both PEs to $-P$. To write $+P$ to both A and B, BL_1 and BL_2 are driven to V_{DD} . In this context, an important aspect needs to be highlighted. When WL is asserted, voltage from BL_1 and BL_2 (which are at V_{DD}) charge D_A (and G_B) and D_B (and G_A). As a result, PeFETs A and B are turned on, while write ensues. This causes D_A and D_B (and connected G_B and G_A) to drop to $V_{DD} - \Delta V$. Reduced gate voltage implies lower V_{GB} across PEs of both PeFETs, which ultimately increase write latency.

2. Read: Currents through BL_1 and BL_2 are sensed after driving them to V_R . WL is asserted with V_{DD} so that both cells get $V_G = V_R$ required for read. GPL and hence LPL of accessed segment is at $0V$ during read. The idea is to have $V_{GB} = \sim V_R$ for both A and B. Depending on whether $+P$ or $-P$ is stored in A (or B), I_{LRS} or I_{HRS} is sensed on BL_1 (or BL_2). As in write, cross-coupling has important effects during read which we elaborate next.

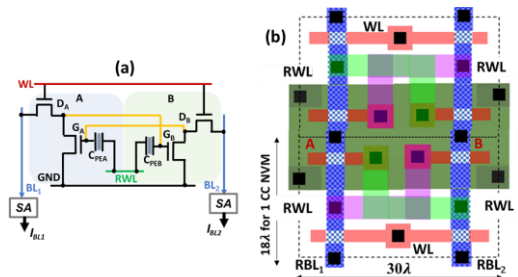


Fig. 8: (a) Schematic and (b) layout of CC NVM.

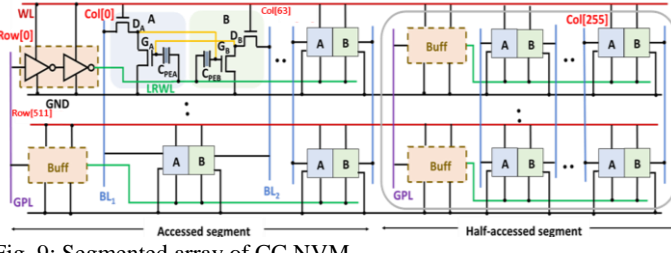


Fig. 9: Segmented array of CC NVM

a. Let, A/B store $-P/-P$. Since both cells are in HRS, D_A and D_B in Fig. 9 is at V_R . Let currents sensed on BL_1/BL_2 be I_{HRS00} .

b. Next, let $-P/+P$ be the stored states of A/B respectively. As A is in HRS, D_A is pulled to V_R as desired. On the other hand, the D_B is pulled down to $V_R - \Delta V$ by action of LRS in cell B. G_A and G_B have similar voltage as D_B and D_A due to cross-coupled connection. So, cell A gets a $V_{GB,A} = V_R - \Delta V < V_R$. This lowered gate voltage makes A (storing $-P$) more resistive than HRS in $-P/-P$ state (previous example) and now we obtain I_{HRS01} on BL_1 which is lesser than I_{HRS00} in (a). For B, G_B is V_R and we obtain I_{LRS01} (with $V_{GB}=V_R$ and $V_{DS}=V_R - \Delta V$) on BL_2 . If A/B has $+P/-P$ instead, we obtain I_{HRS10} on BL_1 and I_{LRS10} on BL_2 .

c. When $+P$ is stored in both PeFETs (i.e., they are in LRS), their drain and connected gate charge to $V_R - \Delta V$. Hence, $V_{GB,A/B} = V_{DS,A/B} = V_R - \Delta V$. Diminished V_{GB} allows lower current (let it be called I_{LRS11}) than I_{LRS10} or I_{LRS01} on BL_1 and BL_2 in this LRS state. Finally, we conclude that $I_{LRS11} < I_{LRS10}$ and $I_{HRS00} > I_{HRS10}$ or I_{HRS01} . We define distinguishability for CC NVM, considering the worst case, as the ratio $-I_{LRS11}/I_{HRS00}$, which is lower than the other PeFET NVMs. Note that in HD and 1T-1PeFET, distinguishability is identical to I_{LRS10}/I_{HRS10} .

While CC NVM exhibits overheads and complex read/write due to cross-coupling, its advantage (as noted earlier) is effective contact sharing lead lower bit area than 1T-1PeFET. Next, we quantify area, performance, energy efficiency of the proposed PeFET NVMs and compare them to 2D-FET SRAMs.

V. ANALYSIS OF PEFET BASED NVM ARRAYS ($\kappa = 0.04$)

A. Layout and area [Fig. 10 (a)]

We use λ (= Gate length/2) based rules and gate/metal pitch defined by Intel 20nm process [24] for layout analysis of PeFET NVMs. In HD NVM, back terminal is shared among adjacent cells in a column (WBL) resulting in a cell height (H) of one poly-pitch ($PP = 9\lambda$). Cell width ($W = 18\lambda$) is controlled by width of PE (dictated by κ as discussed in Section III). Finally, an HD cell's area is $162\lambda^2$. We present tall [Fig. 7(a)] and wide [Fig. 7(b)] layouts for 1T-1PeFET NVM. In the tall variant, we minimize cell area by stacking AX along H . WBL contact (or drain of AX) is shared with adjacent cells in the column. However, sharing of RBL contact is restricted by the internally

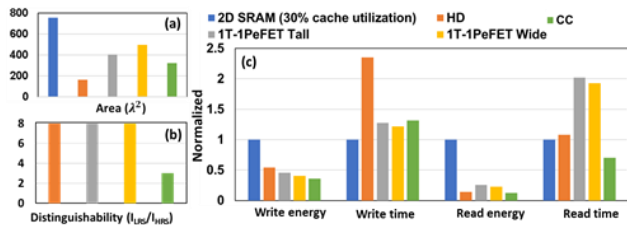
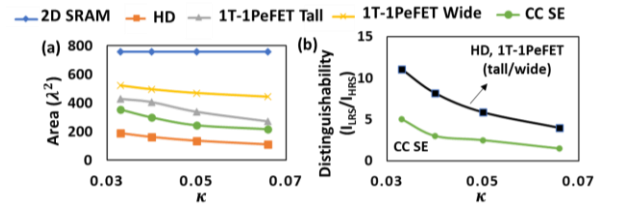


Fig. 10: Analysis of PeFET NVMs compared to 2D-FET SRAM.


 Fig. 11 (a) Area and (b) distinguishability: varying κ

positioned back terminal. Hence, H of 1T-1PeFET tall cell is equal to 2.5 PP (22.5λ) or 2.5X larger footprint than HD. Moreover, we propose wide layout (1T-1PeFET wide NVM) with decreased $H = 2$ PP (18λ) to minimize BL capacitance for improved energy/latency. The κ -dependent width of the back contact and access transistor width including contacts sets W . Its area shows an overhead of 3.1X over HD. Area of CC NVM is 1.4X and 1.7X lower than 1T-1PeFET tall and wide NVM respectively, while it is 1.8X larger than HD cell. Improvement of CC NVM area over 1T-1PeFET is achieved by efficient contact sharing (a) of back contact across PL (along rows unlike in other cells) and (b) of BL with adjacent cells (compare that with limited contact sharing in 1T-1PeFETs). HD, CC, 1T-1PeFET tall and wide NVMs are 4.7X, 2.5X, 1.87X and 1.53X area efficient compared to 2D-FET SRAM.

B. Distinguishability [Fig. 10 (b)]

HD and 1T-1PeFET exhibit same distinguishability ($I_{LRS}/I_{HRS} = 8X$) due to similar strain transduced at a fixed κ . In CC NVM, lower distinguishability of 3X is observed at same κ due to limiting read condition $-I_{LRS10}/I_{HRS10}$ (refer Section IV(E2c)).

C. Write energy and latency [Fig. 10 (c)]

HD NVM shows degraded write energy and latency than other designs due to C_{PE} from half-accessed cells adding to WBL and PL (refer Section IV). In Segmented 1T-1PeFET NVM, AX shields WBL from this capacitance leading to energy and latency improvements over HD. 1T-1PeFET wide design shows minimum latency due to its layout-enabled minimization of BL capacitance. CC NVM combines the benefits of AX (like in 1T-1PeFET) with a smaller area for further write energy optimization. However, it shows higher latency than the 1T-1PeFETs despite its smaller cell area due to P -switching occurring at diminished V_{GB} (described in Section IV). Finally, write energy of HD, Segmented 1T-1PeFET tall, wide and CC NVM is 48%, 56%, 61%, 65% lower than 2D-FET SRAM. Note that these benefits are reported considering 30% utilization [26] for L2 cache. The baseline SRAM cache leaks for the remaining 70% utilization adding leakage energy, whereas PeFET NVMs do not. Large size of SRAM cell along with leakage energy are contributors for its high write energy. Moreover, we observe 22%, 28%, 31% and 134% overhead in latency in 1T-1PeFET wide, tall, CC and HD NVMs (caused by polarization switching) compared to 2D-FET SRAM.

D. Read energy and latency [Fig. 10 (c)]

Among PeFET designs, CC shows minimum read energy as it is compact and PL connected to C_{PE} is not activated during read. HD NVM shows improved read energy than 1T-1PeFET NVMs due smaller RBL capacitance (due to lower layout height) compared to other two designs. Since RBL switching

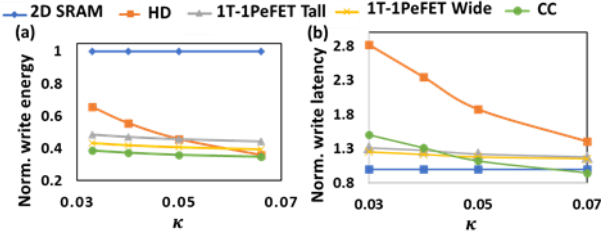


Fig. 12 Write (a) energy and (b) latency: varying κ .

energy is a dominant component of read energy, its reduction affects read energy similarly. We observe lower read energy in PeFET designs than 2D-FET SRAM attributed to (i) negligible leakage and (ii) capability to selectively turn of *RBL* discharge of half-accessed cells during read in PeFET arrays. Note that we access 64 bits during read/write operations for both PeFET and SRAM based arrays for consistency of comparison. Read energy of CC, HD, 1T-1PeFET wide and tall shows 87%, 85%, 77% and 74% improvement respectively compared to 2D-FET SRAM at 30% cache utilization. Impact of C_{PE} during read causes latency to increase in HD, 1T-1PeFET tall and 1T-1PeFET wide by 7%, 93% and 100% compared to 2D-FET SRAM. Contrarily, CC cell shows 30% improvement since C_{PE} is bypassed during read (by keeping *LPL* to 0V).

VI. κ ANALYSIS OF PEFET BASED NVM ARRAYS

We have established in Section III that small κ improves strain transduction to 2D-TMD channel, however at the cost of device footprint. Here, we discuss the effect of κ in NVM array design.

A. Area [Fig. 11(a)]

Increasing κ leads to decrease in cell area of PeFET NVMs. With respect to 2D-FET SRAM, area improvement for PeFET NVM HD ranges from 4X at $\kappa = 0.03$ and to 7X at $\kappa = 0.07$. Size of CC cell is 2.15X-3.5X lower than 2D-FET SRAM for $\kappa = 0.03 - 0.07$. Whereas, 1PeFET tall and wide cells are 1.76X-2.8X and 1.45X-1.71X smaller for $\kappa = 0.03 - 0.07$.

B. Distinguishability [Fig. 11(b)]

The efficiency of strain transduction increases at a lower κ , which boosts distinguishability. For $\kappa=0.03$, it is 11X compared to 3X at $\kappa=0.07$ in HD, 1T-1PeFET tall and wide designs. In CC, it lies in the range of 1.5X - 5X for $\kappa = 0.07 - 0.03$.

C. Write energy and latency [Fig. 12(a, b)]

Write energy and latency of PeFET NVMs improves at higher κ (lower PeFET footprint). Large κ decreases (i) *WL* metal capacitance, and (ii) FE/PE switching capacitance in all PeFET NVMs. In HD, it also reduces C_{PE} of half-accessed cells that adds to *WBL/WL*. Hence, HD exhibits a steeper change in energy/latency with κ . Finally, HD, 1T-1PeFET tall, wide and CC NVM shows up to 36% - 65%, 52% - 56%, 58% - 61% and 62% - 66% improvement in write energy compared to 2D-FET SRAM respectively for $\kappa = 0.03 - 0.07$ (Fig. 12(a)). Write latency overhead over SRAM decreases from 181% (at $\kappa = 0.03$) to 40% (at $\kappa = 0.07$) for HD, 31%-17% for 1T-1PeFET tall, 26%-15% 1T-1PeFET wide designs (Fig. 12 (b)). CC cell shows an improvement of 5% over 2D-FET SRAM at $\kappa = 0.07$.

D. Read energy and latency [Fig. 13(a, b)]

Read energy of all PeFET designs are nearly insensitive to κ . This is because read energy is dominated by *BL* capacitance

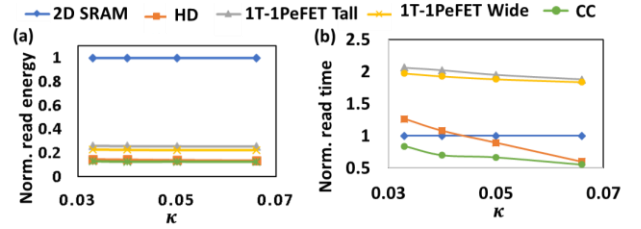


Fig. 13 Read (a) energy and (b) latency: varying κ .

switching energy, which is unaffected by κ [Fig. 13 (a)]. Note by changing κ , we do not change the layout height and hence *RBL* capacitance; we only change the horizontal dimension of the layout. Read latency decreases as κ increases due to smaller cell size and reduced C_{PE} associated with *WL/PL* in HD and 1T-1PeFET designs. HD and CC designs show up to 40% and 44% improvement for $\kappa = 0.07$, whereas the overhead in 1T-1PeFET tall and wide designs decrease to 87% and 83% respectively.

VII. FUTURE OUTLOOK

We have previously elicited the trade-offs between distinguishability, energy and area in PeFET based NVMs. We further proposed device-circuit design techniques to mitigate them, such as, geometry related κ optimization, use of access transistor to design 1T-1PeFET versus access-transistor-less HD, layout optimization of 1T-1PeFET and segmentation in 1T-1PeFET/CC arrays. In the future, we envision that optimization of PeFET based NVMs could be furthered by alternative piezoelectric/ferroelectric materials. For example, Si-doped HfO_2 is a promising replacement for PE material used here - PZT-5H. Recent experiments have pointed to reasonable piezoelectric effects in Si-doped HfO_2 [27]. Moreover, Si-doped HfO_2 ensures good CMOS- compatibility, improved PE thickness scalability, potentially enhanced performance and energy-efficiency of PeFET NVMs. However, information of certain necessary parameters such as elastic tensor components of Si-HfO₂ is currently limited. Advanced characterization for such parameters and understanding endurance limits is required to establish it as the PE material for future PeFETs.

VIII. CONCLUSION

We propose piezoelectric strain FETs (PeFET) utilizing polarization-based bit storage in ferroelectric material, electric field driven write and piezoelectricity induced dynamic bandgap modulation of 2D-TMD channel for bit sensing. We present HD, 1T- 1PeFET tall, wide and CC NVMs based on PeFETs. We analyze them at the array level applying device and circuit optimizations for improved area-energy-latency tradeoff. HD surpasses other PeFET NVMs in compactness with up to 7X smaller area than 2D-FET SRAM. CC NVM stands out with benefits in write energy (66%), read energy (87%) and read latency (44%). However, slower write and weakened distinguishability are its limitations. 1T-1PeFETs are fastest to write, albeit with an overhead over 2D-FET SRAM and show good distinguishability (up to 11X), just as HD.

IX. ACKNOWLEDGMENT

The authors would like to acknowledge Anand Raghunathan and Reena Elangovan (Purdue University) for their inputs.

REFERENCES

- [1] V. Sze, "Designing Hardware for Machine Learning: The Important Role Played by Circuit Designers," *IEEE Solid-State Circuits Magazine*, vol. 9, no. 4, pp. 46–54, Sep. 2017
- [2] P. Gepner and M. F. Kowalik, "Multi-core processors: New way to achieve high system performance," in *PARELEC 2006 - Proceedings: International Symposium on Parallel Computing in Electrical Engineering*, 2006, pp. 9–13.
- [3] D. Apalkov *et al.*, "Spin-transfer torque magnetic random access memory (STT-MRAM)," *ACM Journal on Emerging Technologies in Computing Systems*, vol. 9, no. 2, pp. 1–35, May 2013.
- [4] H.-Y. Chen *et al.*, "Resistive random access memory (RRAM) technology: From material, device, selector, 3D integration to bottom-up fabrication," *Journal of Electroceramics*, vol. 39, no. 1–4, pp. 21–38, Dec. 2017, doi: 10.1007/s10832-017-0095-9.
- [5] B. C. Lee *et al.*, "Phase-Change Technology and the Future of Main Memory," *IEEE Micro*, vol. 30, no. 1, pp. 143–143, Jan. 2010.
- [6] J.-H. Kim *et al.*, "A Highly Reliable FRAM (Ferroelectric Random Access Memory)," in *IEEE International Reliability Physics Symposium Proceedings. 45th Annual*, Apr. 2007, pp. 554–557.
- [7] J. Müller *et al.*, "Ferroelectricity in HfO₂ enables nonvolatile data storage in 28 nm HKMG," in *Digest of Technical Papers - Symposium on VLSI Technology*, 2012, pp. 25–26.
- [8] K. Ni *et al.*, "SoC Logic Compatible Multi-Bit FeMFET Weight Cell for Neuromorphic Applications," in *2018 IEEE International Electron Devices Meeting (IEDM)*, Dec. 2018, pp. 13.2.1-13.2.4
- [9] S. K. Thirumala and S. K. Gunta, "Gate leakage in non-volatile ferroelectric transistors: Device-circuit implications," in *Device Research Conference*, Aug. 2018, vol. 2018-June.
- [10] S. Das, "Two Dimensional Electrostrictive Field Effect Transistor (2D-EFET): A sub-60mV/decade Steep Slope Device with High ON current OPEN," 2016, doi: 10.1038/srep34811.
- [11] M. Peña-Álvarez, E. del Corro, Á. Morales-García, L. Kavan, M. Kalbac, and O. Frank, "Single Layer Molybdenum Disulfide under Direct Out-of-Plane Compression: Low-Stress Band-Gap Engineering," *Nano Letters*, vol. 15, no. 5, pp. 3139–3146, May 2015,
- [12] G. Sun, J. Zhao, M. Poremba, C. Xu, and Y. Xie, "Memory that never forgets: Emerging nonvolatile memory and the implication for architecture design," *National Science Review*, vol. 5, no. 4. Oxford University Press, pp. 577–592, Jul. 01, 2018.
- [13] M. Jerry *et al.*, "A ferroelectric field effect transistor based synaptic weight cell," *Journal of Physics D: Applied Physics*, vol. 51, no. 43, Aug. 2018, doi: 10.1088/1361-6463/aad6f8.
- [14] D. M. News, B. G. Elmegreen, X. H. Liu, and G. J. Martyna, "High response piezoelectric and piezoresistive materials for fast, low voltage switching: Simulation and theory of transduction physics at the nanometer-scale," *Advanced Materials*, vol. 24, no. 27, pp. 3672–3677, Jul. 2012, doi: 10.1002/adma.201104617.
- [15] S. K. Thirumala and S. K. Gunta, "Gate leakage in non-volatile ferroelectric transistors: Device-circuit implications," in *Device Research Conference - Conference Digest, DRC*, Aug. 2018, vol. 2018-June. doi: 10.1109/DRC.2018.8442186.
- [16] M. H. Malakooti and H. A. Sodano, "Noncontact and simultaneous measurement of the d₃₃ and d₃₁ piezoelectric strain coefficients," *Applied Physics Letters*, vol. 102, no. 6, Feb. 2013.
- [17] A. Aziz, S. Ghosh, S. Datta, and S. K. Gupta, "Physics-Based Circuit-Compatible SPICE Model for Ferroelectric Transistors," *IEEE Electron Device Letters*, vol. 37, no. 6, pp. 805–808, Jun. 2016.
- [18] S. v. Suryavanshi and E. Pop, "S2DS: Physics-based compact model for circuit simulation of two-dimensional semiconductor devices including non-idealities," *Journal of Applied Physics*, vol. 120, no. 22. AIP Publishing LLC. doi: 10.1063/1.4971404.
- [19] D. S. Schulman, A. J. Arnold, and S. Das, "Contact engineering for 2D materials and devices," *Chemical Society Reviews*, vol. 47, no. 9. Royal Society of Chemistry, pp. 3037–3058, May 07, 2018.
- [20] Z. Yu *et al.*, "Analyzing the Carrier Mobility in Transition-Metal Dichalcogenide MoS₂ Field-Effect Transistors," *Advanced Functional Materials*, vol. 27, no. 19. Wiley-VCH Verlag, May 18, 2017.
- [21] X. Peng, R. Madler, P. Y. Chen, and S. Yu, "Cross-point memory design challenges and survey of selector device characteristics," *Journal of Computational Electronics*, vol. 16, no. 4, pp. 1167–1174, Dec. 2017, doi: 10.1007/s10825-017-1062-z.
- [22] X. Li *et al.*, "Design of 2T/Cell and 3T/Cell Nonvolatile Memories with Emerging Ferroelectric FETs," *IEEE Design and Test*, vol. 36, no. 3, pp. 39–45, Jun. 2019.
- [23] J. T. Rickes *et al.*, "A novel sense-amplifier and plate-line architecture for ferroelectric memories," *Integrated Ferroelectrics*, vol. 48, pp. 109–118, 2002, doi: 10.1080/713718311.
- [24] "Intel 20nm Lithography." https://en.wikichip.org/wiki/20_nm_lithography_process (accessed Dec. 27, 2021).
- [25] N. Thakuria, D. Schulman, S. Das, and S. K. Gupta, "2-D Strain FET (2D-SFET) Based SRAMs - Part I: Device-Circuit Interactions," *IEEE Transactions on Electron Devices*, vol. 67, no. 11, pp. 4866–4874, Nov. 2020, doi: 10.1109/TED.2020.3022344.
- [26] S P Park, et al. "Future Cache Design using STT MRAMs for Improved Energy Efficiency: Devices, Circuits and Architecture", *Proceedings of the 49th Design Automation Conference: [San Francisco, CA, 3-7 June 2012]*. [IEEE], 2012.
- [27] S. Kirbach, K. Kühnel, and W. Weinreich, "Piezoelectric Hafnium Oxide Thin Films for Energy-Harvesting Applications," in *Proceedings of the IEEE Conference on Nanotechnology*, Jan. 2019, vol. 2018-July. doi: 10.1109/NANO.2018.8626275.